BIOCHEMISTRY
including biophysical chemistry & molecular biology

ARTICLE

pubs.acs.org/biochemistry

Identification of DypB from *Rhodococcus jostii* RHA1 as a Lignin Peroxidase

Mark Ahmad,[†] Joseph N. Roberts,[‡] Elizabeth M. Hardiman,[†] Rahul Singh,[‡] Lindsay D. Eltis,*[,‡] and Timothy D. H. Bugg*[,†]

[†]Department of Chemistry, University of Warwick, Coventry CV4 7AL, U.K.

[‡]Department of Microbiology and Immunology, University of British Columbia, 2350 Health Sciences Mall, Vancouver, British Columbia V6T 1Z3, Canada

Supporting Information

ABSTRACT: *Rhodococcus jostii* RHA1, a polychlorinated biphenyl-degrading soil bacterium whose genome has been sequenced, shows lignin degrading activity in two recently developed spectrophotometric assays. Bioinformatic analysis reveals two unannotated peroxidase genes present in the genome of *R. jostii* RHA1 with sequence similarity to open reading frames in other lignin-degrading microbes. They are members of the Dyp peroxidase family and were annotated as DypA and DypB, on the basis of bioinformatic analysis. Assay of gene deletion mutants using a colorimetric lignin degradation assay reveals that a Δ*dypB* mutant shows greatly reduced lignin degradation activity, consistent with a role in lignin breakdown. Recombinant DypB protein shows activity in the colorimetric assay and shows Michaelis−Menten kinetic behavior using Kraft lignin as a substrate. DypB is activated by Mn^{2+} by 5−23-fold using a range of assay substrates, and breakdown of wheat straw lignocellulose by recombinant DypB is observed over 24−48 h in the presence of 1 mM $MnCl_2$. Incubation of recombinant DypB with a β-aryl ether lignin model compound shows time-dependent turnover, giving vanillin as a product, indicating that $C_\alpha-C_\beta$ bond cleavage has taken place. This reaction is inhibited by addition of diaphorase, consistent with a radical mechanism for C−C bond cleavage. Stopped-flow kinetic analysis of the DypB-catalyzed reaction shows reaction between the intermediate compound I (397 nm) and either Mn^{II} (k_{obs} = 2.35 s^{-1}) or the β-aryl ether (k_{obs} = 3.10 s^{-1}), in the latter case also showing a transient at 417 nm, consistent with a compound II intermediate. These results indicate that DypB has a significant role in lignin degradation in *R. jostii* RHA1, is able to oxidize both polymeric lignin and a lignin model compound, and appears to have both Mn^{II} and lignin oxidation sites. This is the first detailed characterization of a recombinant bacterial lignin peroxidase.

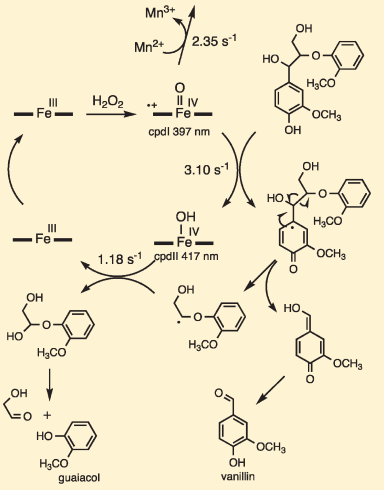

Lignin is a heterogeneous aromatic polymer found as a major component of lignocellulose in plant cell walls and is extremely resistant to chemical and biochemical breakdown. The recalcitrance of the lignin component of lignocellulose is a limitation in the utilization of plant biomass for cellulosic bioethanol generation.[1] Consequently, there is considerable interest in the identification of novel organisms and catalysts for lignin breakdown.

Lignin degradation has been studied primarily in white-rot and brown-rot fungi, which produce extracellular peroxidases and laccases that are able to metabolize lignin.[2] The white-rot fungus *Phanaerochaete chrysosporium* produces a heme-containing lignin peroxidase (LiP)[3] that is able to catalyze the cleavage of lignin model compounds[4,5] and a heme-dependent manganese peroxidase enzyme (MnP) that catalyzes the rapid oxidation of Mn^{II} to Mn^{III}.[6,7] Mn^{III} is then able to oxidize a range of lignin model compounds.[8] *P. chrysosporium* and a range of other fungi also produce extracellular copper-dependent laccase enzymes, which are able to oxidize lignin model compounds, using redox mediators.[9,10] However, despite the study of fungal lignin-degrading enzymes for 25 years, these discoveries have not translated to a commercial process for lignin breakdown, in part because of the inherent difficulties in fungal genetics and protein expression. There are several literature reports of soil bacteria that are able to metabolize lignin;[11,12] however, the enzymology of bacterial lignin degradation is not well characterized. *Streptomyces viridosporus* has been reported to produce extracellular peroxidases,[13] which can metabolize lignin model compounds.[14] Using a radiochemical assay for lignin breakdown, lignin degradation activity has been reported in strains of *Nocardia autotrophica* and *Rhodococcus* sp.[12] However, no bacterial lignin-degrading genes have been identified to date, and no recombinant lignin-degrading enzymes have been characterized.

Received: November 28, 2010
Revised: April 28, 2011
Published: May 02, 2011

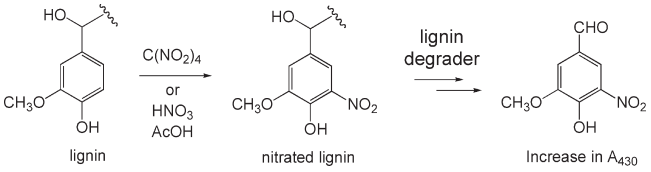

Figure 1. Nitrated lignin assay for monitoring lignin degradation, as described in ref 15.

We have recently reported two spectrophotometric assays for lignin breakdown: an assay involving fluorescently modified lignin and a UV−vis assay involving chemically nitrated lignin (Figure 1), which gives changes in A_{430} upon lignin breakdown, due to production of nitrated phenol products.[15] Using this assay, we have identified several bacterial strains that show lignin degradation activity in their extracellular fraction, including two known aromatic degraders, *Rhodococcus jostii* RHA1 and *Pseudomonas putida* mt-2.[15] These two strains were shown to break down lignocellulose to a low-molecular weight phenolic byproduct.[15] *R. jostii* RHA1 is a degrader of polychlorinated biphenyls (PCBs).[16] The availability of a genome sequence for this organism[17] and the ability to analyze gene function in detail in this organism have prompted us to seek to elucidate the identity of extracellular lignin-degrading enzymes in this organism. Here we report the existence of DyP-type peroxidases DypA and DypB in *R. jostii* RHA1, and the identification of DypB as a lignin peroxidase, the first characterization of a recombinant bacterial lignin peroxidase.

MATERIALS AND METHODS

Materials. The β-aryl ether lignin dimers **1**−**3** were synthesized by the method of Nakatsubo et al.,[18] with the exception that methyl chloroacetate was used instead of ethyl chloroacetate in the first step. (+)-Pinoresinol **4** was purchased from Arbo Nova and used without further purification. *O*-(2-Hydroxyethyl)guaiacol **5** was synthesized by treatment of methyl carboxymethylguaiacol (0.25 g), an intermediate on the synthetic route mentioned above,[18] with $LiAlH_4$ (0.156 g) in tetrahydrofuran (10 mL) at 50 °C for 3 h, followed by addition of wet THF (5 mL), filtration, and evaporation of solvent, to give **5** as a yellow oil (0.225 g, 98%): ^{1}H NMR (300 MHz, $CDCl_3$) δ 6.9−7.0 (4H, m), 4.12 (2H, t, J = 5 Hz), 3.91 (2H, t, J = 5 Hz), 3.85 (3H, s); ^{13}C NMR (75.5 MHz, $CDCl_3$) δ 149.5, 148.0, 121.8, 121.1, 114.2, 111.8, 71.4, 61.2, 55.8; ESI-MS 191.0 ($M\,Na^+$). Milled wood lignin was prepared using a literature procedure.[19] Kraft lignin, *Clostridium kluyveri* diaphorase, and glucose oxidase were purchased from Sigma-Aldrich. HPLC-grade DMSO was from Alfa Aesar. All other reagents and chemicals were purchased from Sigma-Aldrich, ACROS, MP Biomedicals, or Fisher and were used without further purification. Enzymes for molecular cloning were purchased from New England Biolabs.

Phylogenetic Analyses. A structure-based alignment of DyPs was generated using STRAP[20,21] and CLUSTALX2.0.[22] Briefly, the STRAP editor and the TM-Align algorithm[20,21] were used to align the four DyPs with published structures: EfeB of *Escherichia coli* [Protein Data Bank (PDB) entry 2WX6], BtDyp of *Bacteroides thetaiotaomicron* VPI-5482 (PDB entry 2GVK), TyrA of *Shewanella oneidensis* (PDB entry 2HAG), and DyP_{Dec1} (PDB entry 2D3Q). The sequence identities of the DypB homologues to *R. jostii* RHA1 DypA and DypB are 27 and 13% for EfeB, 14 and 23% for TyrA, 13 and 31% for btDyP, and 9 and 9% for DyPDEC1, respectively. The resulting alignment was used as a profile in CLUSTALX 2.0 to align DyP sequences. Initially, all sequences deposited in the Peroxibase database and DyP family sequences found in the literature were considered for this analysis. Sequences were parsed such that none in the final data set were more than 40% identical. Signal sequences, as predicted with SignalP 3.0, were removed from the input sequences.[23] Sequences lacking any one of the conserved residues, Asp153, His226, Arg244, and Asp288 (DypB numbering), or a glutamate in place of an aspartate, were removed from the analysis. The final data set had 39 sequences (Figure S1 of the Supporting Information). For the phylogenetic analyses, the alignment was edited so that it contained only equivalent residues. Accordingly, columns were deleted if they contained insertions, deletions, or residues that were not within 3.0 Å (root-mean-square deviation) of the equivalent residues in each of the superimposed DyP structures. This alignment (Figure S1 of the Supporting Information) served as the input for a maximum-likelihood tree built using PHYLIP version 3.69.[24] Bootstrapping was performed using 100 data sets by jumbling the sequence input order 21 times for each bootstrap and the best tree generated separately by jumbling 21 times.

DNA Manipulation and Plasmid Construction. The *dyp* genes were amplified from fosmid clones RF0013J14 and RF0013A20 containing appropriate fragments of RHA1 genomic DNA (http://www.rhodococcus.ca[17]). The polymerase chain reactions (PCRs) were conducted using Expand High-Fidelity Polymerase (Roche), a Veriti 96-well Thermal Cycler (Applied Biosystems), and the following primers: *dyp*AFor, *dyp*ARev, *dyp*BFor, and *dyp*BRev (Table S1 of the Supporting Information). The amplicons were cloned into pET28a(+) (Novagen) using NdeI and HindIII, yielding pETDYPA1 and pETDYPB1 in which *dypA* and *dypB*, respectively, are under the control of the T7 promoter. The resulting genes encoded recombinant proteins with a cleavable N-terminal poly-His tag (Ht-) and corresponded to residues 50−429 of DypA (i.e., without the TAT signal sequence) and residues 1−350 of DypB.

Construction of the mutagenic plasmid for Δ*dyp*A and Δ*dyp*B genetic knockout strains was designed as described previously using 800−1000 kb amplicons flanking the target gene.[25] The *dyp*A and *dyp*B upstream amplicons were prepared from RHA1 genomic DNA and the following primers: dAUF, dAUR, dBUF, and dBUR (Table S1 of the Supporting Information). These yielded a 790 bp amplicon that included the 5′ 90 bp of *dypA* and 1000 bp amplicon that included the 5′ 99 bp of *dypB*. The downstream amplicons were similarly generated using dADF, dADR, dBDF, and dBDR (Table S1 of the Supporting Information). These yielded amplicons of 999 and 799 bp, respectively, which included the 3′ 99 bp of the respective genes. For *dyp*A or *dyp*B, a three-fragment ligation was performed to clone the flanking amplicons into pK18*mobsac*B, yielding pK18dpA or pK18dpB, respectively. Primer synthesis and nucleotide sequencing of the final clones were performed at the Nucleic Acid-Protein Services Unit (University of British Columbia).

Construction of Mutants. The Δ*dyp*A and Δ*dyp*B deletion mutants of RHA1 were constructed essentially as described previously.[25] Wild-type RHA1 was grown in Lysogeny Broth Peptone medium (LBP) containing 30 μg/mL nalidixic acid at 30 °C for 72 h with shaking. The cultures were subsequently plated on solid LBP agar and incubated for 72 h at 30 °C followed by incubation for 24 h at room temperature. pK18dpA and pK18dpB

were transformed into *E. coli* S17-1 and grown for 24 h on LBP plates supplemented with 25 μg/mL kanamycin at 37 °C. Cells from both the RHA1 and transformed *E. coli* S17-1 plates were resuspended in 2 mL of LBP, and 750 μL aliquots of both strains were mixed carefully. The cell mixture was harvested by centrifugation (9300*g* for 1 min) and resuspended in 1 mL of LBP, and 100 μL aliquots were spread on LBP agar and incubated at 30 °C for 24 h to facilitate conjugation. Biomass was harvested from the plates by resuspension in 2 mL of LBP, and 25 μL aliquots were spread on LBP agar supplemented with 50 μg/mL kanamycin and 30 μg/mL nalidixic acid and incubated at 30 °C to initiate the integration of the pK18*mobsac*B plasmid via a single homologous recombination event. After 72 h, kanamycin resistant colonies (Kan^r) were replica plated on LBP supplemented with 10% (w/v) sucrose and LBP supplemented with 50 μg/mL kanamycin. Both plates contained 30 μg/mL nalidixic acid. Kan^r and sucrose sensitive (Kan^r/Suc^s) colonies were cultured in 25 mL of LBP overnight at 30 °C, and 25 μL aliquots were plated on LBP agar supplemented with 10% (w/v) sucrose. Plates were incubated for 72 h at 30 °C; sucrose resistant (Suc^r) colonies were grown for 24 h at 30 °C following replica plating on LBP agar and LBP agar supplemented with 50 μg/mL kanamycin. Kanamycin sensitive (Kan^s) colonies were screened by colony PCR for truncated *dyp*A and *dyp*B gene products.

Bacterial Strains and Growth. Ht-DypA and DypB were produced in *E. coli* BL21(DE3). Cells containing pETDYPA1 or pETDYPB1 were grown in lysogeny broth (LB)[26] containing 25 μg/mL kanamycin at 37 °C with shaking. Cultures were grown to an OD_{600} of 0.5, at which point isopropyl β-D-thiogalactopyranoside (IPTG) was added to a final concentration of 0.5 mM to induce *dyp* expression. Cells were incubated for a further 12 h at 20 °C while being shaken before being harvested by centrifugation. Pellets were washed three times with 20 mM sodium phosphate and 10% glycerol (pH 8.0) and frozen at −80 °C until they were used.

Protein Purification. Unless otherwise stated, the purification protocol for the DyPs was identical. Approximately 4.5 g of cells (wet weight) was thawed in 20 mL of 20 mM sodium phosphate and 0.1 mM EDTA (pH 8.0) and lysed at 4 °C using an Emulsi Flex-C5 homogenizer (Avestin). Cell debris was removed by centrifugation (140000*g* for 50 min). Ht-DyP was purified from the supernatant using a column with 10 mL of Ni-NTA resin (QIAgen) according to the manufacturer's instructions in the presence of 0.1 mM EDTA. DyP was eluted as the apoprotein from the column and was exchanged into 20 mM 3-(*N*-morpholino)propanesulfonic acid (MOPS) and 80 mM NaCl (pH 7.5) (buffer A) using a 30K NMWL Amicon Ultra-15 Centrifugal Filter Device (Millipore). The affinity tag was removed by incubating the protein with a 200:1 molar ratio of human α-thrombin (Haematologic Technologies Inc.) for 12 h at room temperature, followed by a second IMAC column. The DyPs were eluted from the second IMAC column using buffer A containing 20 mM imidazole and subsequently buffer exchanged into buffer A. As purified, preparations of DypA and DypB had *Rz* values[27] (A_{Soret}/A_{280}) of <0.1. To reconstitute the proteins, hemin chloride was dissolved in DMSO to a final concentration of 20 mg/mL and added dropwise with gentle stirring to protein in buffer A to a final 2:1 hemin:protein molar ratio. Excess hemin was removed via centrifugation followed by gel filtration chromatography using Sephadex G-25 fine (GE Healthcare). Reconstituted DypA and DypB had *Rz* values of 2.7 and 2.9, respectively. The reconstituted DyPs were dialyzed overnight at 4 °C in buffer A containing 1 mM EDTA and were loaded onto 8 mL of Source 15Q anion exchange resin (GE Healthcare) packed in an AP-1 column (Waters Corp., Milford, MA) that had been equilibrated with buffer A and was operated at a flow rate of 3 mL/min. DyPs were eluted using a linear gradient from 80 to 500 mM NaCl in 20 column volumes. The purified protein, which was >95% apparently homogeneous as determined by sodium dodecyl sulfate−polyacrylamide gel electrophoresis, was exchanged into buffer A, concentrated to 20 mg/mL, frozen as beads in liquid nitrogen, and stored at −80 °C until it was used.

UV−Visible Assays. A stock solution of nitrated MWL hereward wheat lignin (0.015 mM) was prepared in 750 mM Tris buffer (pH 7.4) containing 50 mM NaCl. Assays (total volume of 200 μL) were conducted in 96-well Falcon Microtest clear plates, using a TECAN GENios plate reader. To each well were added 30 μL of extracellular cell extract or recombinant protein solution (0.1 mg/mL), 160 μL of nitrated lignin, 10 μL of 40 mM H_2O_2. The absorbance at 430 nm was measured at 1 min intervals for 20 min. Each assay was conducted in duplicate, with controls in which a nitrated lignin or protein solution was replaced with 750 mM Tris (pH 7.4) containing 50 mM NaCl. Assays of recombinant DypA and DypB were also conducted in the presence of 30 μL of 50 mM $MnCl_2$. The whole plate was repeated without addition of H_2O_2. All readings were taken in duplicate.

Kinetic Analysis of DypB with Kraft Lignin. In a 1 mL cuvette, Kraft lignin (500 μL, 0.5 mg/mL), succinate buffer (175 μL, pH 5.5, 50 mM), $MnCl_2$ (200 μL, 50 mM), DypB (25 μL, 1 mg/mL), and hydrogen peroxide (100 μL, 40 mM) were mixed in the order stated, and the absorbance was monitored for 5−10 min at 465 nm. Substrate concentrations were then varied for $MnCl_2$ (final concentration of 1.25−10 mM) and Kraft lignin (final concentration of 0.05−0.25 mg/mL), with the total volume kept at 1.0 mL. The molar concentration of Kraft lignin was calculated using an average molecular mass of 10000 Da.

Incubation of DypB with Lignocellulose and Lignin. Powdered wheat straw lignocellulose or milled wood lignin (5 mg) was added to succinate buffer (3 mL, 50 mM, pH 5.5), and then DypB (100 μL, 1 mg/mL) was added, followed by H_2O_2 (100 mL, 40 mM). The resulting solution was incubated at 30 °C for 48 h. Aliquots (1 mL) were taken at 1, 3, 5, 24, and 48 h. These fractions were analyzed by HPLC. Aliquots for HPLC (400 μL) were mixed with CCl_3COOH (100%, w/v, 40 μL), and the solution was then centrifuged for 4 min at 10000 rpm. The experiment was also repeated with hydrogen peroxide replaced with glucose (final concentration of 0.3 mM) and glucose oxidase (final concentration of 0.5 mg/mL). Both experiments were conducted with and without $MnCl_2$ (1 mM). HPLC analysis was conducted using a Phenomenex Luna 5 μm C_{18} reverse phase column (100 Å, 50 mm × 4.6 mm) on a Hewlett-Packard Series 1100 analyzer, at a flow rate of 0.5 mL/min, with monitoring at 310 nm. The gradient was as follows: 20 to 30% MeOH/H_2O over 5 min, 30 to 50% MeOH/H_2O from 5 to 12 min, and 50 to 80% MeOH/H_2O from 12 to 25 min.

Reaction of DypB with Lignin Model Compounds. Samples of lignin model compounds (all three types of β-aryl ether, pinoresinol) (2 mL, 5 mM solution in a 9:1 acetone/water mixture) were diluted with succinate buffer (3 mL, 50 mM, pH 5.5), and then DypB (25 μL, 1 mg/mL) and $MnCl_2$ (100 μL, 50 mM) were added, followed by H_2O_2 (100 μL, 40 mM). The resulting solution was incubated at 30 °C for 48 h. Aliquots (1 mL) were taken at 1, 3, 5, 24, and 48 h. These fractions were analyzed by HPLC, gas chromatography and mass spectroscopy

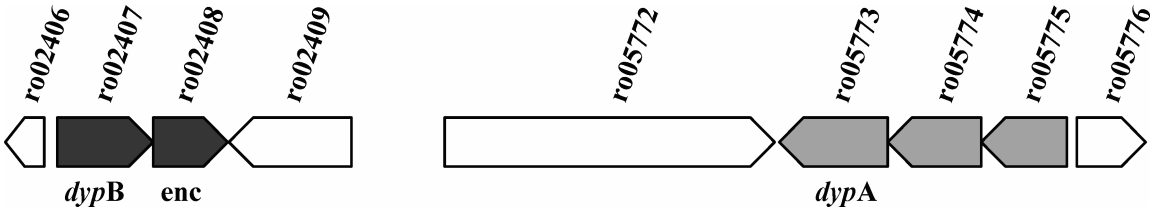

Figure 2. Operonic structure of *dypA* and *dypB* in *R. jostii* RHA1.

(GC−MS), and liquid chromatography and mass spectroscopy (LC−MS). Aliquots for HPLC (400 μL) were mixed with CCl_3COOH (100%, w/v, 40 μL) and centrifuged (13000 rpm for 5 min) prior to analysis. Samples for GC−MS (200 μL) were extracted into HPLC-grade ethyl acetate (1 mL) and then *N,O*-bis(trimethylsilyl)acetamide (200 μL) and (chlorotrimethlyl)-silane (10 μL). The solution was left for 1 h and then diluted 100-fold in the same solvent prior to injection. For each model compound, a control in which no DypB was added was run. In the case of β-aryl ether **2**, the hydrogen peroxide was also replaced with glucose oxidase (final concentration of 0.5 mg/mL) and glucose (final concentration of 0.3 mM), and the reaction was repeated without $MnCl_2$. This reaction was repeated in the presence of *C. kluyveri* diaphorase (0.5 mL, 2 mg/mL), with or without NADH (2 mL, 5 mM stock). LC−MS analysis was conducted using a Phenomenex Luna 5 μm C_{18} reverse phase column (100 Å, 50 mm × 4.6 mm) on an Agilent 1200 instrument, at a flow rate of 0.5 mL/min, with a Bruker HCT Ultra mass spectrometer. The LC gradient was as follows: 20 to 30% MeOH/H_2O over 5 min, 30 to 50% MeOH/H_2O from 5 to 12 min, and 50 to 80% MeOH/H_2O from 12 to 25 min.

Stopped-Flow Kinetic Analysis. Kinetic measurements were taken with a MOS 450-Biologic spectrophotometer and an SFM 300 observation chamber equipped with a 1 cm observation cell at 25 °C, monitoring at a fixed wavelength. Recombinant DypB (8 μM) was prepared in 30 mM citrate/60 mM phosphate buffer (pH 6.0) and mixed with freshly prepared solutions of hydrogen peroxide, $MnCl_2$, and β-aryl ether **2** at 8 or 80 μM. All measurements were taken in triplicate. The decay of DypB compound I was observed at 397 nm (DOI 10.1021/bi200427h). The decay of compound II was observed at 417 nm, which is the isosbestic point between compound II and the resting enzyme.[7] Kinetic transients were fitted to single- and double-exponential kinetic models, and in most cases, good fits to single-exponential functions were observed.

RESULTS

Identification of *dyp* Genes by Bioinformatic Analysis. As a starting point for bioinformatic analysis, we examined the genome of *Nocardia farcinica*, closely related to *Nocardia autotrophica*, which has been found to show activity for lignin degradation,[15,16] for peroxidase genes of unknown function. *N. farcinica* contains three unannotated peroxidase genes (GenBank accession numbers Q5YV75, Q5YZF4, and Q5YPL4). Searches using the BLAST algorithm revealed that Q5YPL4 shared homologues in *Streptomyces coelicolor* (GenBank accession number Q9FBY9, 66% identical), *Mycobacterium tuberculosis* (GenBank accession number A0R4G9, 63% identical), *Pseudomonas fluorescens* (GenBank accession number Q4KA97, 56% identical), *R. jostii* RHA1 (GenBank accession number Q0SE24, 52% identical), and *Zymomonas mobiliz* (GenBank accession number Q5NM63, 55% identical).

Table 1. Annotation of DyPs and Proteins Encoded by Predicted Cotranscribed Genes in the RHA1 Genome

gene ID	annotation	BeTs[a] to characterized homologues	percent identity (%)[b]
ro02407	DypB	BtDyp of *Bacteroides thetaiotaomicron* VPI-5482	41
ro02408	encapsulin	Encapsulin of *Thermotoga maritima*	34
ro05773	DypA	EfeB of *E. coli* K-12	32
ro05774	lipoprotein	EfeO of *E. coli* K-12	35
ro05775	Fe^{II}/Pb^{II} permease	EfeU of *E. coli* K-12	27

[a] Best hits from a local alignment of the NCBI database. [b] Based on full-length alignment.

The gene identified in *R. jostii* RHA1 (ro02407) encodes a 350-amino acid peroxidase (M_r = 37222), a member of the DyP peroxidase family, that shows high activity toward dye substrates and contains a distal aspartic acid proton donor.[28−30] Two putative DyPs were encoded in the RHA1 genome. These were named DypA and DypB on the basis of the phylogenetic analysis below. To gain insight into the identity and function of the predicted RHA1 DyPs, we employed local alignments to explore the *dyp* genes and their genomic context (Figure 2). The predicted DypA protein is 32% identical in amino acid sequence to EfeB from *E. coli* K-12, also known as YcdB in strain O157:H7 (Table 1). In *E. coli*, this gene belongs to the efeUOB operon involved in Fe^{2+} uptake under acidic conditions.[31] Consistent with this finding, EfeB has a twin-arginine transport (TAT) signal sequence, EfeO possesses an N-terminal cupredoxin domain, and EfeU is a homologue of the high-affinity iron permease FTR1 from *Saccharomyces cerevisiae*.[32] The efeUOB operon is conserved in RHA1 (Figure 2 and Table 1), and DypA is predicted to contain a TAT signal sequence, suggesting that it is exported.

Among characterized homologues, DypB is 41% identical in amino acid sequence to BtDyP, whose crystal structure has been determined.[30] The *dyp*B gene is predicted to be operonically coupled with ro02408, annotated here as *enc* as its gene product is 34% identical to encapsulin from *T. maritima*, which forms a cellular nanocompartment (Figure 2).[11] Moreover, the RHA1 DypB is predicted to contain the C-terminal sequence responsible for targeting proteins for encapsulation.[33]

Phylogenetic Analysis. The four DyP structures available in the PDB were superimposed using STRAP to guide the sequence alignment. The associated TM-score for the four aligned sequences exceeded 0.75, with overall root-mean-square deviation (rmsd) values ranging from 3.1 to 3.2 Å, consistent with the

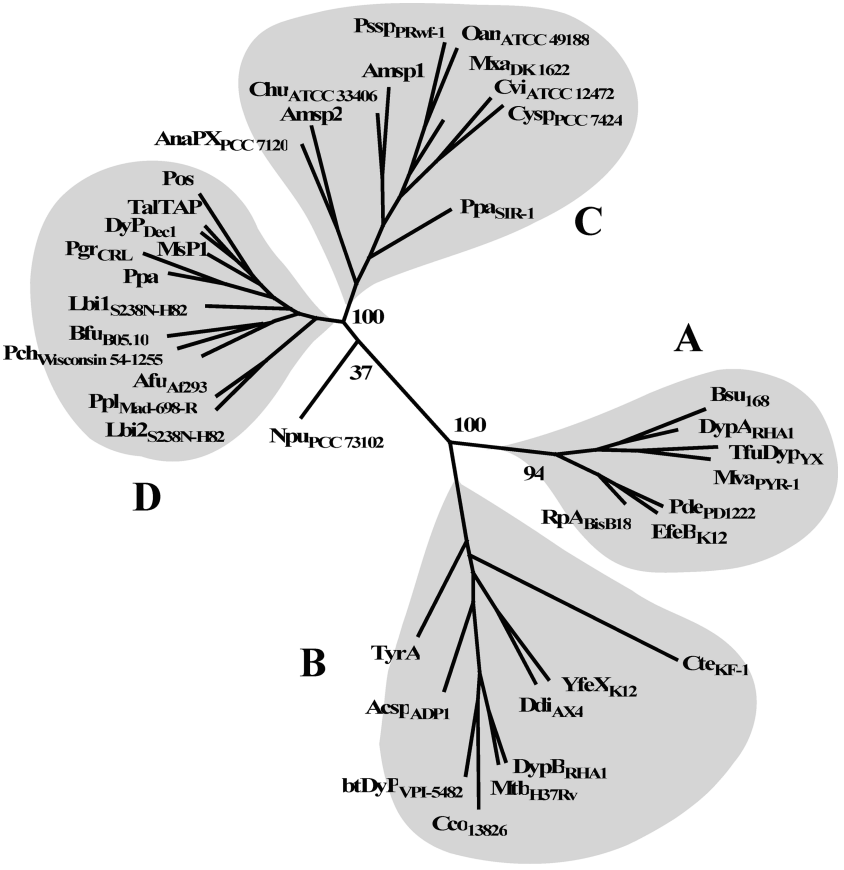

Figure 3. Radial phylogram of DyPs. The names of bacterial or fungal strains are indicated in subscript with the protein or abbreviated organism names. Structure-based sequence alignments were performed using EfeB$_{K-12}$ from *E. coli* K-12 (2WX6), TyrA from *S. oneidensis* (2HAG), BtDyP$_{VPI-5482}$ from *B. thetaiotaomicron* VPI-5482 (2GVK), DyP$_{DEC1}$ from *Thanatephorus cucumeris* DEC1 (2D3Q), DypA$_{RHA1}$ and DypB$_{RHA1}$ from *R. jostii* RHA1 (ABG97551.1 and ABG94212.1, respectively), YfeX$_{K-12}$ from *E. coli* K-12 (BAE76711.1), AnaPX$_{PCC\ 7120}$ from *Anabaena* sp. PCC 7120 (BAB77951.1), TfuDyp$_{YX}$ from *Thermobifida fusca* YX, MsP1 from *Marasmius scorodonius*, TalTAP from *Termitomyces albuminosus*, Bsu$_{168}$ from *Bacillus subtilis* 168 (CAB15852.1), Mva$_{PYR-1}$ from *Mycobacterium vanbaalenii* PYR-1 (ABM12972.1), Pde$_{PD1222}$ from *Paracoccus denitrificans* PD1222 (ABL69832.1), RpA$_{BisB18}$ from *Rhodopseudomonas palustris* BisB18 (ABD87513.1), Cte$_{KF-1}$ from *Comamonas testosteroni* KF-1 (EED66859.1), Ddi$_{AX4}$ from *Dictyostelium discoideum* AX4 (EAL70759.1), Mtb$_{H37Rv}$ from *M. tuberculosis* H37Rv (CAB09574.1), Cco$_{13826}$ from *Campylobacter concisus* 13826 (EAT98288.1), Acsp$_{ADP1}$ from *Acinetobacter* sp. ADP1 (CAG67144.1), Ppa$_{SIR-1}$ from *Plesiocystis pacifica* SIR-1 (EDM76509.1), Cysp$_{PCC\ 7424}$ from *Cyanothece* sp. PCC 7424 (ACK71272.1), Cvi$_{ATCC\ 12472}$ from *Chromobacterium violaceum* ATCC 12472 (AAQ59612.1), Mxa$_{DK\ 1622}$ from *Myxococcus xanthus* DK 1622 (ABF90727.1), Oan$_{ATCC\ 49185}$ from *Ochrobactrum anthropi* ATCC 49185 (ABS17389.1), Pssp$_{PRwf-1}$ from *Psychrobacter* sp. PRwf-1 (ABQ94167.1), Chu$_{ATCC\ 33406}$ from *Cytophaga hutchinsonii* ATCC 49185 (ABG59511.1), Pos from *Pleurotus ostreatus* (CAK55151.1), Pgr$_{CRL}$ from *Puccinia graminis* CRL (AAWC01001299.1), Ppa from *Phakopsora pachyrhizi*, Lbi1$_{S238N-H82}$ and Lbi2$_{S238N-H82}$ from *Laccaria bicolor* S238N-H82 (ABFE01001782.1 and EDR12662.1, respectively), Bfu$_{B05.10}$ from *Botryotinia fuckeliana* B05.10 (EDN26366.1), Pch$_{Wisconson\ 54-1255}$ from *Penicillium chrysogenum* Wisconson 54-1255 (CAP99029.1), Afu$_{Af293}$ from *Aspergillus fumigatus* Af293 (EAL86784.2), Ppl$_{Mad-698-R}$ from *Postia placenta* Mad-698-R (EED79944.1), and Amsp1 and Amsp2 from *Amycolatopsis* sp. (personal communication with M. Chang, University of California, Berkeley, CA). As described in Materials and Methods, the structure-based alignment included only equivalent residues. The tree was calculated using protein maximum likelihood. Bootstrap values of critical nodes are indicated.

shared ferredoxin-like structural fold of these proteins. The TM-align superposition further indicated that the four DyPs have 234 equivalent residue positions. After the alignment of the parsed set of collected DyP sequences with the structural alignment profile, a total of 39 sequences were retained in the final alignment (Figure S1 of the Supporting Information). For the phylogenetic analyses, only the structurally equivalent residues were maintained in the alignment, corresponding to an average of 55% of each sequence (Figure S1 of the Supporting Information). Chlorite dismutase, a heme-containing enzyme with the same structural fold as DyP,[30] was excluded from the alignment as the TM-scores were below 0.6, the overall rmsd values ranged from 3.5 to 3.8 Å, and the enzyme lacks the distal aspartate of DyPs.[34]

Using a maximum likelihood analysis, the DyP sequences were grouped into four discrete subfamilies (Figure 3). These were identified as A−D to be consistent with a previous analysis.[35] The four DyPs for which structural data are available belong to subfamilies A, B, and D. Subfamilies A and B, which are grouped within the phylogram, comprise bacterial DyPs. Subfamilies C and D, which are also grouped together, comprise bacterial and fungal sequences, respectively. The most divergent of the analyzed DyPs are 6% identical in sequence. Within subfamilies, this value is 15%. RHA1 DypA and DypB were named according to the subfamilies in which they were grouped.

Analysis of Gene Deletion Mutants. Deletion mutants of *R. jostii* RHA1 in genes *dypA* and *dypB* were prepared, using the method of van der Geize et al.[25] The culture supernatant from

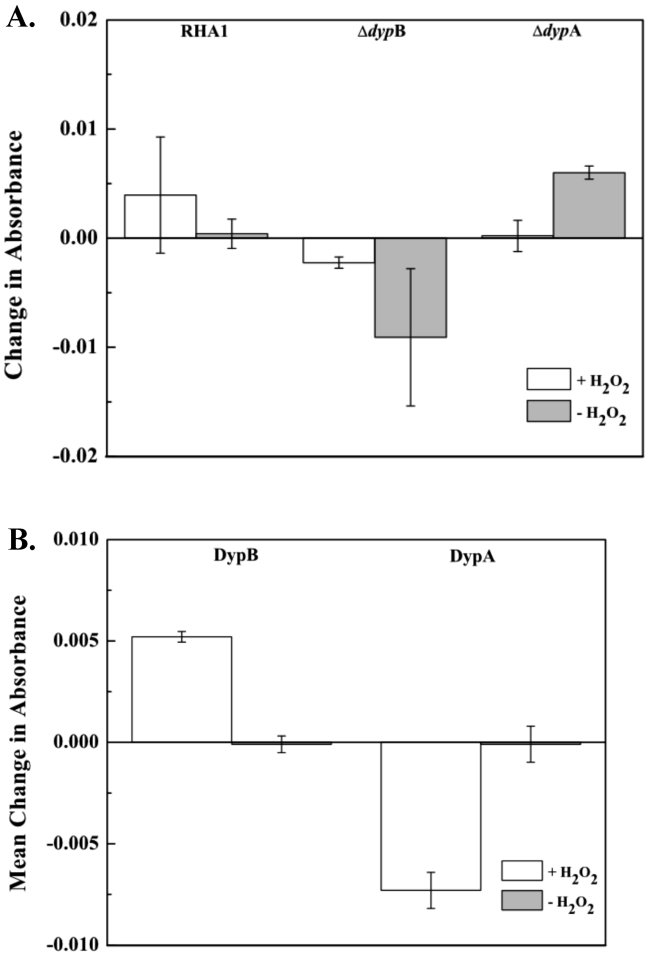

Figure 4. Activities of *R. jostii* RHA1 gene deletion strains and DypA and DypB recombinant enzymes using the nitrated lignin UV−vis assay. (A) Activity (change in absorbance at 430 nm) in the nitrated lignin UV−vis assay of the culture supernatant obtained from wild-type RHA1 and Δ*dypB* and Δ*dypA* gene deletion mutants, in the presence (white) and absence (gray) of 2 mM hydrogen peroxide. (B) Activity (change in absorbance over a 20 min assay) of 25 μg of recombinant DypA and DypB protein in the nitrated lignin UV−vis assay, in the presence (white) or absence (gray) of 2 mM hydrogen peroxide.

the mutant strains was examined for lignin degradation activity using the previously described nitrated lignin UV−vis assay.[15] Although this assay shows some experimental scatter using cell supernatant, we have previously found that lignin-degrading strains show an increase in absorbance at 430 nm, relative to controls, whereas nondegraders show a zero or negative value.[15] As shown in Figure 4, wild-type *R. jostii* RHA1 shows hydrogen peroxide-dependent activity, as observed previously,[15] whereas the Δ*dypB* strain shows no observable activity in the presence or absence of hydrogen peroxide and a significant decrease in activity compared to that of the wild-type strain. The Δ*dypA* strain exhibited a slightly lower activity than the wild-type strain. These data provide some evidence of a role for the *dypB* gene in the ability of *R. jostii* RHA1 to break down lignin but are inconclusive with regard to the role of the *dypA* gene.

Kinetic Evaluation of Recombinant DypA and DypB. Recombinant DypA and DypB proteins were expressed in *E. coli* as His_6 fusion proteins, purified by affinity chromatography, and reconstituted with heme, as described in Materials and Methods. Both proteins were found to exhibit peroxidase activity using ABTS as a substrate (DOI 10.1021/bi200427h). Using ABTS as a substrate, the optimal activity for DypB was observed at pH 3.6, but activity was retained at pH 5−6. Each protein was tested in the nitrated lignin UV−vis assay,[15] in the presence and absence of 2 mM hydrogen peroxide. As shown in Figure 5, DypB exhibited activity in the presence of hydrogen peroxide, but not in the absence of hydrogen peroxide. Under the same conditions, DypA exhibited no activity, in the presence or absence of hydrogen peroxide. These data therefore support the conclusions of the earlier gene knockout experiments, implying that DypB shows activity as a lignin peroxidase but DypA does not. DypB was found to show 5.4-fold greater activity in this assay in the presence of 1 mM $MnCl_2$ (see Table 2), suggesting that Mn^{2+} acts as a cofactor or mediator for DypB. Using the ABTS assay, DypB showed 8.5-fold higher activity in the presence of 1 mM $MnCl_2$ (see Table 2), and a specific activity of 4.8 μmol min^{-1} (mg of protein)$^{-1}$ was calculated using ABTS as a substrate.

To evaluate further its lignin-degrading activity, recombinant DypB was then assayed against samples of lignin and lignocellulose. When 25 μg of recombinant DypB was incubated at 30 °C with 5 mg of wheat straw lignocellulose in 50 mM succinate buffer (pH 5.5) for 48 h, in the presence of either 2 mM hydrogen peroxide or 0.3 mM glucose and 1.5 mg of glucose oxidase, no changes were observed in the reverse phase HPLC chromatograms of the culture supernatant. However, incubation of DypB in the presence of 1 mM $MnCl_2$ with wheat straw lignocellulose, 0.3 mM glucose, and 1.5 mg of glucose oxidase led to time-dependent changes in the reverse phase HPLC chromatograms of the aliquots that had been removed. As shown in Figure 5, a peak at 17 min disappeared in 1−3 h, while peaks at 19.8 and 21.8 min disappeared over 24−48 h, consistent with breakdown. Although the identity of these peaks is not known, the time-dependent changes were not observed in the absence of $MnCl_2$ or DypB; moreover, similar time-dependent changes are observed upon incubation of *R. jostii* RHA1 with lignocellulose, and no changes are observed in the presence of nondegrading *Ba. subtilis*.[15] A similar incubation experiment conducted using wheat straw milled wood lignin as a substrate also resulted in time-dependent changes by reverse phase HPLC over 24−48 h (data not shown). These experiments indicate that recombinant DypB can, under certain conditions, react with a polymeric lignin substrate.

DypB was also incubated with samples of commercially available Kraft lignin, an industrially produced byproduct of paper manufacturing. When Kraft lignin was incubated in the presence of 1−10 mM $MnCl_2$, monitoring of the reaction by UV−vis spectroscopy versus time revealed a time-dependent change in the UV−vis spectrum at 465 nm in a 10 min assay. Control experiments in the absence of lignin gave a <10% change in absorbance, indicating that the observed change was due to reaction with lignin, rather than oxidation of Mn^{II} to Mn^{III}. Rate measurements at this wavelength at a range of $MnCl_2$ and Kraft lignin concentrations were found to follow saturation kinetics (Figure S2 of the Supporting Information). The deduced apparent K_m value for $MnCl_2$ is 8.4 mM. Using the average M_r value of 10000 for commercial Kraft lignin, an apparent K_m value of 20 μM can be calculated for Kraft lignin; however, this value may not be meaningful, because the substrate is heterogeneous, and the enzyme may interact with only a part of the lignin substrate.

To examine the reaction of DypB with different possible lignin substructures, we then assayed recombinant DypB against a

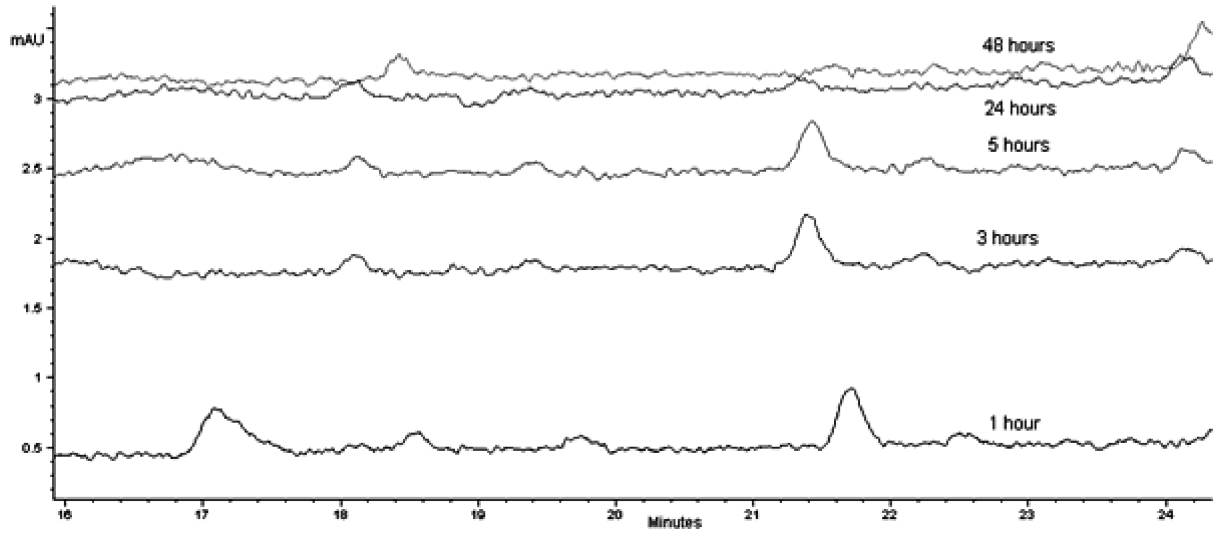

Figure 5. Changes vs time in the reverse phase HPLC chromatogram of an incubation of recombinant DypB with wheat straw lignocellulose. Twenty-five micrograms of recombinant DypB was incubated at 30 °C with 5 mg of wheat straw lignocellulose in 50 mM succinate buffer (pH 5.5) for 48 h, in the presence of 0.3 mM glucose and 1.5 mg of glucose oxidase, and 1 mM $MnCl_2$; aliquots were analyzed by reverse phase HPLC, as described in Materials and Methods, with UV detection at 310 nm.

Table 2. Activation of DypB by $MnCl_2$, Using Different Steady-State Assay Methods, with Polymeric or Small Molecule Substrates

		without $MnCl_2$		with $MnCl_2$		
substrate	assay method	with substrate	without substrate	with substrate	without substrate	*x*-fold activation
nitrated lignin	UV−vis[a]	0.0015	<0.001	0.0081	0.0025	5.4
Kraft lignin	UV−vis[b]	0.039	ND[f]	0.24	0.010	6.2
ABTS	UV−vis[c]	0.0065	<0.0005	0.0549	<0.002	8.5
β-aryl ether **2**	HPLC[d]	0.0023	ND[f]	0.053	ND[f]	23
lignocellulose	HPLC[e]	0% after 24 h		100% after 24 h		

[a] Change in absorbance at 430 nm in a 20 min assay, with 1 μg of protein and 1 mM $MnCl_2$. [b] Change in absorbance at 465 nm in a 10 min assay, with 3 μg of protein and 1.5 mM $MnCl_2$. [c] Change in absorbance per minute at 430 nm, with 1 μg of protein, 0.5 mM $MnCl_2$, and 10 mM ABTS in 50 mM sodium acetate buffer (pH 5.0). [d] Disappearance of the HPLC peak vs time (millimoles per cubic decimeter per hour), with 2 μg of protein and 1 mM $MnCl_2$. [e] Percent disappearance of the 17 min HPLC peak after incubation for 24 h, with 100 μg of protein in 50 mM succinate buffer (pH 5.5) and 1 mM $MnCl_2$. [f] Not determined.

series of lignin model compounds, synthesized according to established literature methods (see Materials and Methods), in the presence of 2 mM hydrogen peroxide. Three different β-aryl ether model compounds were tested at a concentration of 2 mM (the *p*-hydroxy analogue **1**, the guaicyl analogue **2**, and the syringyl analogue **3**), as well as pinoresinol **4**. Each substrate was incubated with DypB at a concentration of 2 mM, and the reaction was analyzed by reverse phase HPLC over 1−5 h. Gradual consumption of guaicyl β-aryl ether **2** was observed, to the extent of 20−30% peak height over 5 h (Figure S3 of the Supporting Information), but no turnover was detected with the other substrates. By monitoring the rate of disappearance of **2** by HPLC versus time, we determined specific activities for the *erythro* and *threo* isomers of **2**. Values of 0.017 μmol min^{-1} (mg of protein)$^{-1}$ for the *erythro* isomer and 0.005 μmol min^{-1} (mg of protein)$^{-1}$ for the *threo* isomer were calculated.

Investigation of Reaction Products of Recombinant DypB with β-Aryl Ether 2. The turnover of β-aryl ether **2** by DypB allowed a more detailed study of the molecular site of action and catalytic mechanism of DypB. The reaction products from incubation of β-aryl ether **2** with DypB were analyzed by LC−MS. A broad envelope of product peaks was observed, found by LC−MS to give peaks in the range of m/z 400−800, higher than the molecular weight of the starting material **2**, therefore indicating the likelihood that recombination of radical products was taking place, to give higher-molecular weight species. The expected C_α−C_β bond cleavage reaction, shown in Figure 6, should release guaiacol as a product: no guaiacol was observed directly; however, a peak at a retention time of 27 min showed an ion at m/z 407, consistent with a guaiacol trimer (MK^+ 407), and the same species was formed upon incubation of guaiacol with DypB.

To probe the existence of radical intermediates in the mechanism of this transformation, the reaction of DypB with **2** was repeated in the presence of *C. kluyveri* diaphorase, known to be involved in free radical defense.[36] In the presence of 0.4 mg/mL diaphorase and 0.8 mM NADH, no reaction products were observed, implying that the cleavage reaction had been completely inhibited. In the presence of 0.4 mg/mL diaphorase but without added NADH, several additional products were observed.

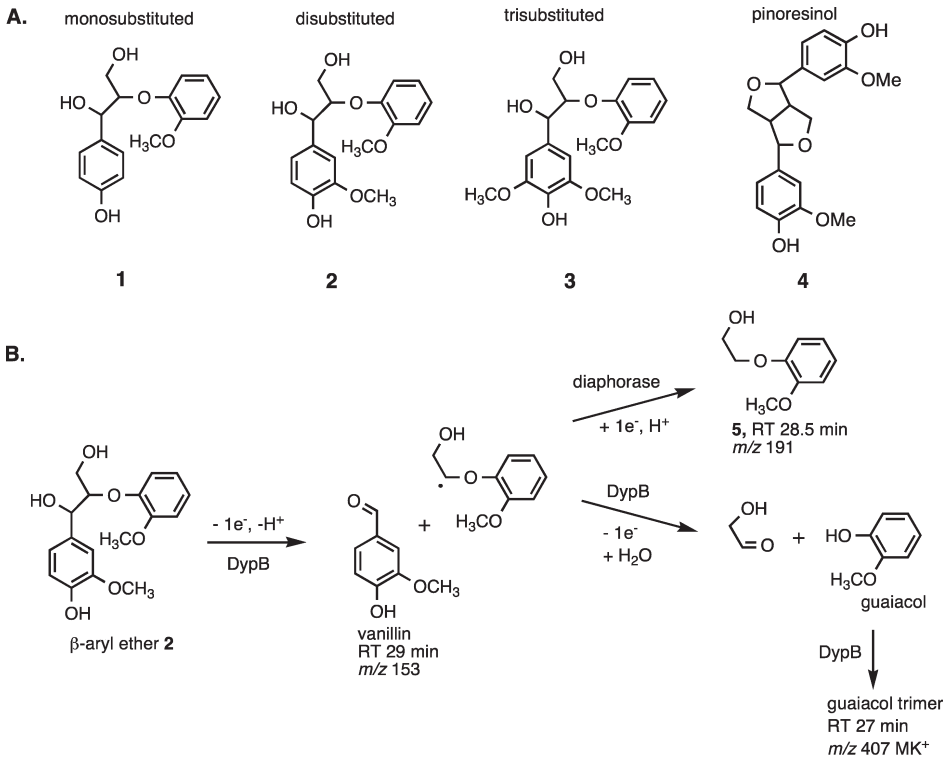

Figure 6. A. Structures of lignin model compounds tested as substrates for DypB. B. Expected and observed products from $C_\alpha-C_\beta$ bond cleavage of β-aryl ether **2** by DypB. HPLC and LC−MS data for reaction of DypB with β-aryl ether **2** are shown in Figures S3−S7 of the Supporting Information.

Selected ion monitoring at m/z 153 for product vanillin revealed a small peak with a retention time of 28.4 min, with the same retention time and molecular ion (m/z 153.2 MH^+) as an authentic sample of vanillin. The observed peak for vanillin was small; however, separate studies have shown that vanillin is itself oxidized by peroxidase DypB (see below). A peak was observed with a retention time of 28.6 min at m/z 191.0, which matched the expected molecular weight of the reduced $C_\alpha-C_\beta$ bond fragment **5**, whose structure is shown in Figure 7. An authentic standard for this alcohol was synthesized by $LiAlH_4$ reduction of methyl carboxymethyl guaiacol (see Materials and MethodsExperimental Procedures), and the standard gave a retention time and a mass spectrum identical to those of the peak formed by DypB and **2** (Figure S4 of the Supporting Information). The guaiacol trimer was again observed in this experiment. Therefore, LC−MS data have been obtained to support each of the expected cleavage products (see Figure 7) formed by $C_\alpha-C_\beta$ bond cleavage of **2** by DypB.

Role of Mn^{II} in DypB Catalysis. We have observed using several different assays that DypB activity is enhanced by Mn^{2+} (see Table 2). By analogy with the fungal lignin-degrading peroxidases, DypB might therefore be a manganese peroxidase, whose primary role is to oxidize Mn^{II} to Mn^{III}.[6,7] A third class of peroxidase, typified by *Pleurotus eryngii* versatile peroxidase, oxidizes Mn^{II} and lignin at comparable rates.[37] To distinguish between these possibilities, the reaction rates of DypB-catalyzed oxidation of Mn^{II} versus lignin must be compared directly, which can be achieved using stopped-flow UV−vis spectrophotometry. In the following paper (DOI 10.1021/bi200427h), a stable compound I-like intermediate species has been characterized for DypB, with a λ_{max} of 397 nm. Therefore, the rates of oxidation

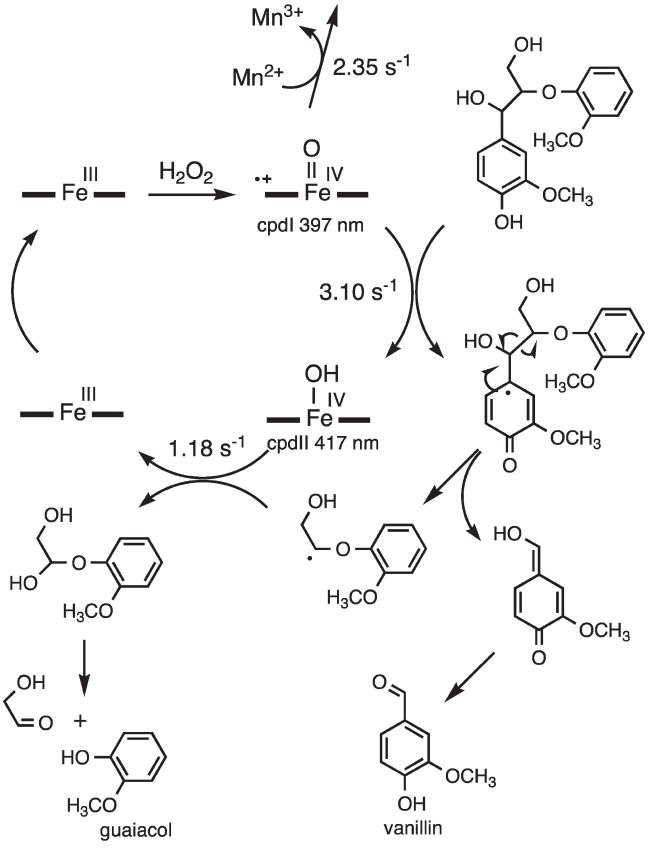

Figure 7. Catalytic cycle of DypB, showing pathways and rate constants for turnover of β-aryl ether **2**, to generate vanillin, or reaction with Mn^{II}.

Table 3. Stopped-Flow Kinetic Data for DypB, Recorded at 397 nm (compound I) or 417 nm (compound II)[a]

	397 nm		417 nm	
conditions	amplitude	k_{obs} (s^{-1}) (χ^2)	amplitude	k_{obs} (s^{-1}) (χ^2)
1:1 DypB:H_2O_2	7.4×10^{-3}	0.84 (5.0×10^{-4})	2.3×10^{-3}	1.01 (4.3×10^{-4})
1:1:1 DypB:H_2O_2:$MnCl_2$	6.3×10^{-3}	2.35 (4.2×10^{-4})	*b*	
1:1:1 DypB:H_2O_2:β-aryl ether	6.1×10^{-3}	3.10 (5.9×10^{-4})	7.5×10^{-3}	1.18 (5.7×10^{-4})
1:1:1:1 DypB:H_2O_2:$MnCl_2$:β-aryl ether	7.6×10^{-3}	2.81 (5.2×10^{-4})		
1:1:10 DypB:H_2O_2:$MnCl_2$	8.3×10^{-3}	1.99 (4.9×10^{-4})		
1:1:10 DypB:H_2O_2:β-aryl ether	6.3×10^{-3}	2.11 (6.2×10^{-4})		
	-1.8×10^{-3}	0.38		

[a] Experiments were conducted as described in Meterials and Methods, using 8 μM DypB and 1 or 10 equiv of hydrogen peroxide, $MnCl_2$, or β-aryl ether **2**, at pH 6.0 and 25 °C. In each case, the transient kinetic data were fit to a single exponential (except the final row) where the data gave a better fit to a two-step process. The individual data sets are shown in Figures S10−S15 of the Supporting Information. [b] Transient not observed.

of β-aryl ether **2** and Mn^{II} by DypB were measured via stopped-flow UV−vis spectrophotometry.

A series of stopped-flow experiments were conducted with recombinant DypB, mixing 8 μM enzyme in citrate/phosphate buffer (pH 6.0) with 1 equiv of hydrogen peroxide and 1 or 10 equiv of $MnCl_2$ and/or β-aryl ether **2**, and monitoring the reaction either at 397 nm (for compound I) or 417 nm (for compound II), and the data are listed in Table 3. When the sample was mixed with only hydrogen peroxide, a first-order decay of compound I (k_{obs} = 0.84 s^{-1}) was observed at 397 nm, because of the breakdown of compound I. Addition of 1 equiv of either $MnCl_2$ (k_{obs} = 2.35 s^{-1}) or β-aryl ether **2** (k_{obs} = 3.10 s^{-1}) gave first-order transients with higher k_{obs} values, consistent with a reaction of DypB compound I with either Mn^{II} or lignin model compound **2**. No significant change in k_{obs} was found with an increase in the ratio of $MnCl_2$ or β-aryl ether **2** to DypB from 1:1 to 10:1 (see Table 3). Single-electron oxidation of Mn^{II} or β-aryl ether by compound I should generate a compound II intermediate, observed in other peroxidases at 417 nm.[7] Observation at 417 nm revealed a first-order transient when DypB was mixed with 1 equiv of hydrogen peroxide and β-aryl ether **2** (k_{obs} = 1.18 s^{-1}), but no change at 417 nm was detected upon mixing with $MnCl_2$ (see Table 3).

As noted above, conversion of β-aryl ether **2** by DypB gave rise to little or no vanillin product; therefore, we suspected that vanillin could be oxidized by DypB, which was verified by pre-steady-state kinetics. Incubation of 8 μM DypB with 1 mM vanillin was found to give a 4-fold acceleration in the k_{obs} for the reaction of compound I at 397 nm and pH 5.5 and 7.5 (Figure S2 of the Supporting Information). In this case, we did not observe a compound II-like intermediate during the reaction of compound I.

DISCUSSION

The microbial degradation of lignin has been studied mainly in white-rot and brown-rot fungi, with the assumption that bacteria are unable or slow to degrade lignin. However, there are several reports of bacteria that have lignin degrading ability,[11,12] and we have previously identified a group of lignin-degrading bacteria, including *R. jostii* RHA1, that have activity comparable to that of some lignin-degrading fungi.[15] There are reports of extracellular peroxidases in *St. viridosporus* that are able to metabolize lignin model compounds, but no protein sequence data are available for these enzymes.[14] The identification of bacterial lignin-degrading genes would allow the high-level overexpression of the corresponding enzymes, and possible protein engineering and pathway engineering approaches for lignin breakdown; hence, we have undertaken the identification of lignin-degrading enzymes in *R. jostii* RHA1.

We have used a bioinformatics approach to identify two DyP-type peroxidases in *R. jostii* RHA1 that have homologues in other lignin-degrading bacteria, for which spectroscopic and kinetic characterization is presented in the following paper (DOI 10.1021/bi200427h). The phylogenetic analyses of DyP peroxidases confirm and extend previous studies. Using only a sequence-based alignment and neighbor joining methods, DyPs had been classified into four discrete subfamilies, A−D.[35] As in our analysis, subfamilies A−C were classified as bacterial while subfamily D was classified fungal, consistent with the Peroxibase database.[38] However, our analysis reclassifies some DyPs. For example, the cyanobacterial AnaPX[35] appears to be a C-type enzyme. The similarity between A- and B-type DyPs on one hand with C and D types on the other has been disputed because of their low levels of sequence identity.[39] However, the current TM-align superposition establishes the homology of the DyPs through their common structural fold and conserved active site residues.

Gene deletion studies show that a Δ*dypB* deletion mutant of *R. jostii* RHA1 has greatly impaired activity for lignin breakdown, whereas a Δ*dypA* deletion mutant is unimpaired, compared with wild-type RHA1. Expression of recombinant DypA and DypB proteins and the nitrated lignin UV−vis assay have confirmed that DypB shows activity in the presence of hydrogen peroxide, which is enhanced in the presence of $MnCl_2$, whereas DypA does not. DypB also shows Michaelis−Menten kinetic behavior with samples of Kraft lignin, shows effects upon lignocellulose breakdown in the presence of $MnCl_2$, and accepts a β-aryl ether lignin model compound as a synthetic substrate. Taken together, these data indicate that peroxidase DypB is involved in lignin breakdown by *R. jostii* RHA1. The turnover of only the disubstituted β-aryl ether **2**, and not the other lignin model compounds, suggests that DypB is quite selective in its lignin degrading activity. The cellular role of the DypA enzyme may be iron uptake or utilization, because molecular genetic evidence has recently been published for the deferrochelation of heme iron by the DyP homologues in *E. coli*.[40] Indeed, of 111 unique A-type DyP genes in the BioCyc database,[41] 86% are predicted to have a TAT signal sequence and 90% are encoded by genes that are clustered with those predicted to encode iron uptake proteins.

The activation of DypB by Mn^{II} ions is reminiscent of the fungal manganese peroxidase, whose rate of oxidation of Mn^{II} to Mn^{III} is much faster than its rate of oxidation of lignin model compounds.[6,7] Activation of DypB by Mn^{II} was observed using several different assays and substrates (see Table 2), and the presence of Mn^{II} was found to be necessary to metabolize lignocellulose, implying that Mn^{II} can act as an oxidative mediator for DypB. Nevertheless, Mn^{II} is a relatively poor substrate for DypB-catalyzed oxidation, with a k_{cat}/K_m value 10^4-10^5-fold lower than that observed with fungal Mn peroxidases (DOI 10.1021/bi200427h). Moreover, the observation of Michaelis−Menten kinetic behavior of Kraft lignin suggests that DypB may be able to bind lignin (or some part of the lignin structure) as part of its catalytic reaction.[a] To examine whether DypB oxidizes Mn^{II} in preference to β-aryl ether **2**, we have studied these reactions using pre-steady-state kinetics. The kinetic data in Table 3 indicate a faster reaction of compound I in the presence of Mn^{II} or β-aryl ether **2**, but only modest increases in k_{obs} were found; only in the case of β-aryl ether **2** was a compound II species observed at 417 nm. These data are not consistent with DypB acting as a Mn peroxidase, in which case much higher rates would be expected in the presence of Mn^{II}. There is some evidence of turnover of β-aryl ether **2** via a one-electron oxidation mechanism, consistent with the inhibition of turnover by diaphorase. The increases in k_{obs} in the presence of substrate are modest, suggesting that DypB is not a highly active peroxidase, but it is possible that β-aryl ether **2** may not be the optimal substrate. The behavior of DypB is more reminiscent of that of the *Pl. eryngii* versatile peroxidase, which has both manganese peroxidase and lignin peroxidase interaction sites.[37] In the following paper (DOI 10.1021/bi200427h), a putative manganese binding site is identified in the crystal structure of RHA1 DypB.

We have identified using LC−MS the reaction products from turnover of β-aryl ether **2** by DypB. The observation of a complex mixture of higher-molecular weight reaction products, and the inhibition of this reaction by diaphorase, are consistent with a radical cleavage mechanism. In the presence of diaphorase, we have identified vanillin and guaiacol derivative **5** as products, indicating that $C_\alpha-C_\beta$ bond cleavage is taking place, as found for the fungal Mn peroxidase.[8] Because DypB also shows activity toward guaiacol and vanillin as substrates (data not shown), the mechanism is likely to proceed via one-electron oxidation of the phenolic ring, followed by C−C bond cleavage, as shown in Figure 7. We did not detect guaiacol itself in this experiment, but we did observe a species corresponding to a guaiacol trimer, also formed upon reaction of DypB with guaiacol as the substrate; therefore, our interpretation is that guaiacol is formed from **2** but is then rapidly oxidized by further reaction with DypB.

The cellular location of DypB must logically be extracellular, because the sample used for our UV−vis assay is the extracellular protein fraction after centrifugation. However, the protein sequence for *R. jostii* RHA1 DypB contains neither a Sec signal sequence nor a TAT signal sequence. Interestingly, most DypA homologues contain predicted TAT signal sequences, but most DypB homologues do not. Immediately adjacent to the *dypB* gene (ro02407) in the RHA1 genome is the ro02408 gene, predicted to encode an encapsulin protein that has been shown to form an icosahedral nanocompartment.[33] Sutter et al. have identified a C-terminal peptide tag that is found in proteins that associate with encapsulin,[33] and this C-terminal tag is found in RHA1 DypB. A survey of the BioCyc database[41] revealed that 14% of the 150 B-type *dyp* genes are predicted to be co-operonic with the encapsulin gene. The operonic coupling of the DyP and encapsulin genes appears to occur only in burkholderials and actinomycetales. It therefore seems probable that the targeting of RHA1 DypB is somehow achieved with the aid of the adjacent encapsulin gene, though the precise mechanism of this process remains to be determined. Interestingly, members of the encapsulin family have been identified in the supernatants of mycobacterial cell cultures.[42]

In conclusion, we have identified a novel manganese-dependent lignin peroxidase DypB, which plays a significant role in lignin degradation by *R. jostii* RHA1. Considering that the in vitro activity of recombinant DypB with lignocellulose is quite modest, we suspect that there is a group of oxidative enzymes used by the host for lignin metabolism, of which DypB is only one member. Nevertheless, it is the first recombinant bacterial lignin peroxidase to be kinetically characterized. The identification of DypB and further bacterial lignin-degrading enzymes, and their availability in recombinant form, will provide valuable new reagents for the conversion of lignocellulose to biofuels and renewable chemicals.

■ ASSOCIATED CONTENT

Supporting Information. Sequences of oligonucleotide primers (Table S1), alignment of Dyp protein sequences (Figure S1), steady-state kinetic data for reaction of DypB with Kraft lignin (Figure S2); HPLC and LC−MS data for reaction of DypB with β-aryl ether **2** (Figures S3−S7), and stopped-flow kinetic data for reaction of DypB with hydrogen peroxide, $MnCl_2$, and β-aryl ether **2** (Figures S8−S15). This material is available free of charge via the Internet at http://pubs.acs.org.

■ AUTHOR INFORMATION

Corresponding Author

*Department of Chemistry, University of Warwick, Coventry CV4 7AL, U.K. Telephone: 44-(0)2476-573018. Fax: 44-(0)2476-524112. E-mail: T.D.Bugg@warwick.ac.uk.

Author Contributions

M.A. and J.N.R. contributed equally to the research.

Funding Sources

This work was supported by research grants from the BBSRC IBTI Biorefinery Club (Grant BB/H004270/1) and the Innovative Materials Research Centre, University of Warwick, and a Natural Sciences and Engineering Research Council (NSERC) of Canada Discovery grant (to L.D.E.). J.N.R. was the recipient of an NSERC studentship.

Notes

[a] A reviewer has pointed out that the saturation kinetic behavior observed with Kraft lignin, which is surprising, could perhaps be caused by a physical phenomenon such as aggregation of the substrate above a threshold level.

■ ACKNOWLEDGMENT

We thank Jie Liu for skilled technical assistance.

■ ABBREVIATIONS

PCB, polychlorinated biphenyl; ABTS, 2,2′-azinobis(3-ethylbenzthiazoline-6-sulfonic acid); LiP, lignin peroxidase; MnP,

manganese peroxidase; DyP, dye-decolorizing peroxidase; TAT, twin-arginine transport; LBP, lysogeny broth peptone; MWL, milled wood lignin; HPLC, high-performance liquid chromatography.

REFERENCES

(1) Sustainable biofuels: Prospects and challenges, Report by the Royal Society, January 2008.

(2) Wong, D. W. S. (2009) Structure and action mechanism of lignolytic enzymes. *Appl. Biochem. Biotechnol. 157*, 174–209.

(3) Tien, M., and Kirk, T. K. (1984) Lignin-degrading enzyme from *Phanerochaete chrysosporium*: Purification, characterization, and catalytic properties of a unique H_2O_2-requiring oxygenase. *Proc. Natl. Acad. Sci. U.S.A. 81*, 2280–2284.

(4) Hammel, K. E., Tien, M., Kalyanaraman, B., and Kirk, T. K. (1984) Mechanism of oxidative C_α-C_β cleavage of a lignin model dimer by *Phanerochaete chrysosporium* ligninase: Stoichiometry and involvement of free radicals. *J. Biol. Chem. 260*, 8348–8353.

(5) Miki, K., Renganathan, V., and Gold, M. H. (1986) Mechanism of β-aryl ether dimeric lignin model compound oxidation by lignin peroxidase of *Phanerochaete chrysosporium*. *Biochemistry 25*, 4790–4796.

(6) Glenn, J. K., Akileswaran, L., and Gold, M. H. (1986) Mn(II) oxidation is the principal function of the extracellular Mn peroxidase from *Phanerochaete chrysosporium*. *Arch. Biochem. Biophys. 251*, 688–696.

(7) Wariishi, H., Dunford, H. B., MacDonald, I. D., and Gold, M. H. (1989) Manganese peroxidase from the lignin-degrading basidomycete *Phanerochaete chrysosporium*: Transient state kinetics and reaction mechanism. *J. Biol. Chem. 264*, 3335–3340.

(8) Tuor, U., Wariishi, H., Schoemaker, H. E., and Gold, M. H. (1992) Oxidation of phenolic arylglycerol β-aryl ether lignin model compounds by manganese peroxidase from *Phanerochaete chrysosporium*: Oxidative cleavage of an α-carbonyl model compound. *Biochemistry 31*, 4986–4995.

(9) Kawai, S., Umezawa, T., and Higuchi, T. (1988) Degradation mechanisms of phenolic β-1 lignin substructure model compounds by laccase of *Coriolus versicolor*. *Arch. Biochem. Biophys. 262*, 99–110.

(10) Bourbonnais, R., Paice, M. G., Freiermuth, B., Bodie, E., and Borneman, S. (1997) Reactivities of various mediators and laccases with Kraft pulp and lignin model compounds. *Appl. Environ. Microbiol. 63*, 4627–4632.

(11) Vicuna, R. (1988) Bacterial degradation of lignin. *Enzyme Microb. Technol. 10*, 646–655.

(12) Zimmermann, W. (1990) Degradation of lignin by bacteria. *J. Biotechnol. 13*, 119–130.

(13) Crawford, D., Pometto, A., III, and Crawford, R. (1983) Lignin degradation by *Streptomyces viridosporus*: Isolation and charaterization of a new polymeric lignin degradation intermediate. *Appl. Environ. Microbiol. 45*, 898–904.

(14) Ramachandra, M., Crawford, D., and Hertel, G. (1988) Characterization of an extracellular lignin peroxidase of the lignocellulolytic actinomycete *Streptomyces viridosporus*. *Appl. Environ. Microbiol. 54*, 3057–3063.

(15) Ahmad, M., Taylor, C. R., Pink, D., Burton, K., Eastwood, D., Bending, G. D., and Bugg, T. D. H. (2010) Development of novel assays for lignin degradation: Comparative analysis of bacterial and fungal lignin degraders. *Mol. BioSyst. 6*, 815–821.

(16) Seto, M., Kimbara, K., Shimura, M., Hatta, T., Fukuda, M., and Yano, K. (1995) A novel transformation of polychlorinated biphenyls by *Rhodococcus* sp. strain RHA1. *Appl. Environ. Microbiol. 61*, 3353–3358.

(17) McLeod, M. P., Warren, R. L., Hsiao, W. W. L., Araki, N., Myhre, M., Fernandes, C., Miyazawa, D., Wong, W., Lillquist, A. L., Wang, D., Dosanjh, M., Hara, H., Petrescu, A., Morin, R. D., Yang, G., Stott, J. M., Schein, J. E., Shin, H., Smailus, D., Siddiqui, A. S., Marra, M. A., Jones, S. J. M., Holt, R., Brinkman, F. S. L., Miyauchi, K., Fukuda, M., Davies, J. E., Mohn, W. W., and Eltis, L. D. (2006) The complete genome of *Rhodococcus* sp. RHA1 provides insights into a catabolic powerhouse. *Proc. Natl. Acad. Sci. U.S.A. 103*, 15582–15587.

(18) Nakatsubo, F., Sato, K., and Higuchi, H. (1975) Synthesis of guaiacyldlycerol-β-guaiacyl ether. *Holzforschung 29*, 165–168.

(19) Zimmermann, W., Paterson, A., and Broda, P. (1988) Conventional and high-performance size-exclusion chromatography of graminaceous lignin carbohydrate complexes. *Methods Enzymol. 161*, 191–199.

(20) Zhang, Y., and Skolnick, J. (2005) TM-align: A protein structure alignment algorithm based on the TM-score. *Nucleic Acids Res. 33*, 2302–2309.

(21) Gille, C., and Frommel, C. (2001) STRAP: Editor for STRuctural Alignments of Proteins. *Bioinformatics 17*, 377–378.

(22) Larkin, M. A., Blackshields, G., Brown, N. P., Chenna, R., McGettigan, P. A., McWilliam, H., Valentin, F., Wallace, I. M., Wilm, A., Lopez, R., Thompson, J. D., Gibson, T. J., and Higgins, D. G. (2007) Clustal W and clustal X version 2.0. *Bioinformatics 23*, 2947–2948.

(23) Bendtsen, J. D., Nielsen, H., von Heijne, G., and Brunak, S. (2004) Improved prediction of signal peptides: SignalP 3.0. *J. Mol. Biol. 340*, 783–795.

(24) Felsenstein, J. (1989) Phylip: Phylogeny inference package (version 3.2). *Cladistics 5*, 164–166.

(25) van der Geize, R., Hessels, G. I., van Gerwen, R., van der Meijden, P., and Dijkhuizen, L. (2001) Unmarked gene deletion mutagenesis of *kstD*, encoding 3-ketosteroid Δ^1-dehydrogenase, in *Rhodococcus erythropolis* SQ1 using *sacB* as counter-selectable marker. *FEMS Microbiol. Lett. 205*, 197–202.

(26) Bertani, G. (2004) Lysogeny at mid-twentieth century: P1, P2, and other experimental, systems. *J. Bacteriol. 186*, 595–600.

(27) Falk, J. E. (1964) *Porphyrins and metalloporphyrins; their general, physical and coordination chemistry, and laboratory methods*, Elsevier Publishing Co., Amsterdam.

(28) Sugano, Y., Muramatsu, R., Ichiyanagi, A., Sato, T., and Shoda, M. (2007) DyP, a unique dye-decolorizing peroxidase, represents a novel heme peroxidase family: Asp-171 replaces the distal histidine of classical peroxidases. *J. Biol. Chem. 282*, 36652–36658.

(29) Zubieta, C., Krishna, S. S., Kapoor, M., Kozbial, P., McMullan, D., Axelrod, H. L., Miller, M. D., Abdubek, P., Ambing, E., Astakhova, T., Carlton, D., Chiu, H. J., Clayton, T., Deller, M. C., Duan, L., Elsliger, M. A., Feuerhelm, J., Grzechnik, S. K., Hale, J., Hampton, E., Han, G. W., Jaroszewski, L., Jin, K. K., Klock, H. E., Knuth, M. W., Kumar, A., Marciano, D., Morse, A. T., Nigoghossian, E., Okach, L., Oommachen, S., Reyes, R., Rife, C. L., Schimmel, P., van den Bedem, H., Weekes, D., White, A., Xu, Q., Hodgson, K. O., Wooley, J., Deacon, A. M., Godzik, A., Lesley, S. A., and Wilson, I. A. (2007) Crystal structures of two novel dye-decolorizing peroxidases reveal a β-barrel fold with a conserved heme-binding motif. *Proteins 69*, 223–233.

(30) Zubieta, C., Joseph, R., Krishna, S. S., McMullan, D., Kapoor, M., Axelrod, H. L., Miller, M. D., Abdubek, P., Acosta, C., Astakhova, T., Carlton, D., Chiu, H. J., Clayton, T., Deller, M. C., Duan, L., Elias, Y., Elsliger, M. A., Feuerhelm, J., Grzechnik, S. K., Hale, J., Han, G. W., Jaroszewski, L., Jin, K. K., Klock, H. E., Knuth, M. W., Kozbial, P., Kumar, A., Marciano, D., Morse, A. T., Murphy, K. D., Nigoghossian, E., Okach, L., Oommachen, S., Reyes, R., Rife, C. L., Schimmel, P., Trout, C. V., van den Bedem, H., Weekes, D., White, A., Xu, Q., Hodgson, K. O., Wooley, J., Deacon, A. M., Godzik, A., Lesley, S. A., and Wilson, I. A. (2007) Identification and structural characterization of heme binding in a novel dye-decolorizing peroxidase, TyrA. *Proteins 69*, 234–243.

(31) Cao, J., Woodhall, M. R., Alvarez, J., Cartron, M. L., and Andrews, S. C. (2007) EfeUOB (YcdNOB) is a tripartite, acid-induced and CpxAR-regulated, low-pH Fe^{2+} transporter that is cryptic in *Escherichia coli* K-12 but functional in *E-coli* O157:H7. *Mol. Microbiol. 65*, 857–875.

(32) Stearman, R., Yuan, D. S., Yamaguchi-Iwai, Y., Klausner, R. D., and Dancis, A. (1996) A permease-oxidase complex involved in high-affinity iron uptake in yeast. *Science 271*, 1552–1557.

(33) Sutter, M., Boehringer, D., Gutmann, S., Günther, S., Prangishvili, D., Loessner, M. J., Stetter, K. O., Weber-Ban, E., and Ban, N. (2008) Structural basis of enzyme encapsulation into a bacterial nanocompartment. *Nat. Struct. Mol. Biol. 15*, 939–947.

(34) de Geus, D. C., Thomassen, E. A., Hagedoorn, P. L., Pannu, N. S., van Duijn, E., and Abrahams, J. P. (2009) Crystal structure of

chlorite dismutase, a detoxifying enzyme producing molecular oxygen. *J. Mol. Biol. 387*, 192–206.

(35) Ogola, H. J. O., Kamiike, T., Hashimoto, N., Ashida, H., Ishikawa, T., Shibata, H., and Sawa, Y. (2009) Molecular characterization of a novel peroxidase from the cyanobacterium *Anabaena* sp. strain PCC 7120. *Appl. Environ. Microbiol. 75*, 7509–7518.

(36) Beyer, R. E., Segura Aguilar, J., Di Bernardo, S., Cavazzoni, M., Fato, R., Fiorentini, D., Galli, M. C., Setti, M., Jandi, L., and Lenaz, G. (1996) The role of DT-diaphorase in the maintenance of the reduced antioxidant form of coenzyme Q in membrane systems. *Proc. Natl. Acad. Sci. U.S.A. 93*, 2528–2532.

(37) Camarero, S., Sarkar, S., Ruiz-Duenas, F. J., Martinez, M. J., and Martinez, A. T. (1999) Description of a versatile peroxidase involved in the natural degradation of lignin that has both manganese peroxidase and lignin peroxidase substrate interaction sites. *J. Biol. Chem. 274*, 10324–10330.

(38) Koua, D., Cerutti, L., Falquet, L., Sigrist, C. J., Theiler, G., Hulo, N., and Dunand, C. (2009) PeroxiBase: A database with new tools for peroxidase family classification. *Nucleic Acids Res. 37*, D261–D266.

(39) Hofrichter, M., Ullrich, R., Pecyna, M. J., Liers, C., and Lundell, T. (2010) New and classic families of secreted fungal heme peroxidases. *Appl. Microbiol. Biotechnol. 87*, 871–897.

(40) Letoffe, S., Heuck, G., Delepelaire, P., Lange, N., and Wandersman, C. (2009) Bacteria capture iron from heme by keeping tetrapyrrol skeleton intact. *Proc. Natl. Acad. Sci. U.S.A. 106*, 11719–11724.

(41) Karp, P. D., Ouzounis, C. A., Moore-Kochlacs, C., Goldovsky, L., Kaipa, P., Ahren, D., Tsoka, S., Darzentas, N., Kunin, V., and Lopez-Bigas, N. (2005) Expansion of the BioCyc collection of pathway/genome databases to 160 genomes. *Nucleic Acids Res. 33*, 6083–6089.

(42) Rosenkrands, I., Rasmussen, P. B., Carnio, M., Jacobsen, S., Theisen, M., and Andersen, P. (1998) Identification and characterization of a 29-kilodalton protein from *Mycobacterium tuberculosis* culture filtrate recognized by mouse memory effector cells. *Infect. Immun. 66*, 2728–2735.